

Figure 4: Variation of  $\Delta A_{CP}$  with the pseudo-rapidity of the reconstructed  $D^{*\pm}$ . The data are divided into 8 disjoint bins and the value of  $\Delta A_{CP}$  measured in each bin. The red dashed line shows the result for the combined sample.

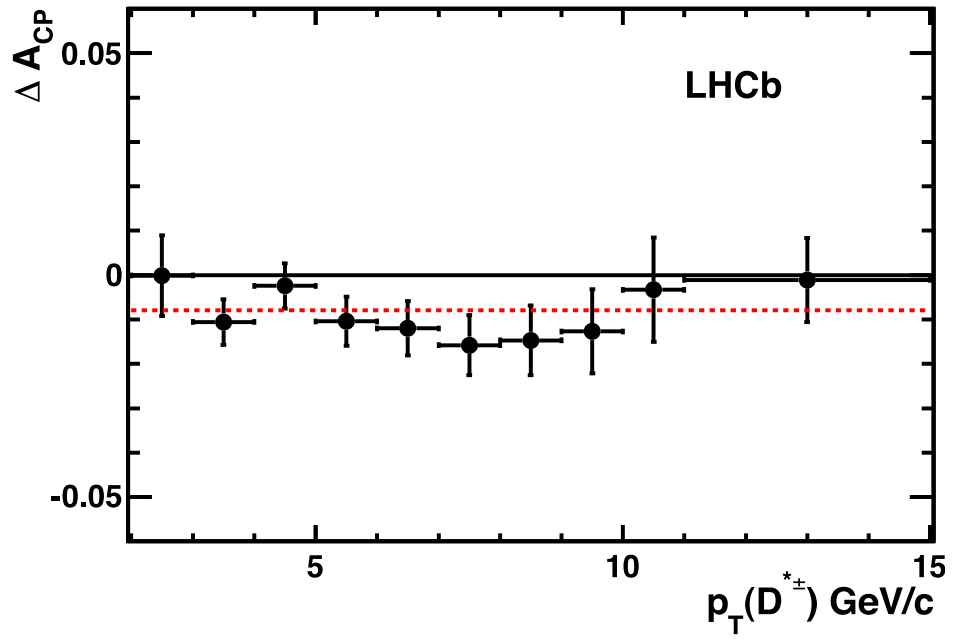


Figure 5: Variation of  $\Delta A_{CP}$  with the transverse momentum of the reconstructed  $D^{*\pm}$ . The data are divided into 10 disjoint bins and the value of  $\Delta A_{CP}$  measured in each bin. The red dashed line shows the result for the combined sample.

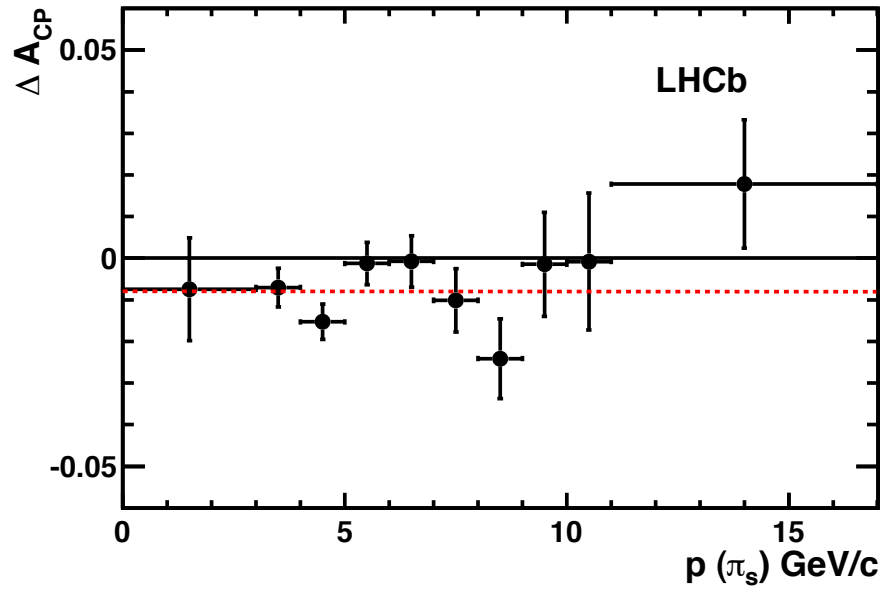


Figure 6: Variation of  $\Delta A_{CP}$  with the momentum of the reconstructed slow pion ( $\pi_s$ ). The data are divided into 10 disjoint bins and the value of  $\Delta A_{CP}$  measured in each bin. The red dashed line shows the result for the combined sample.

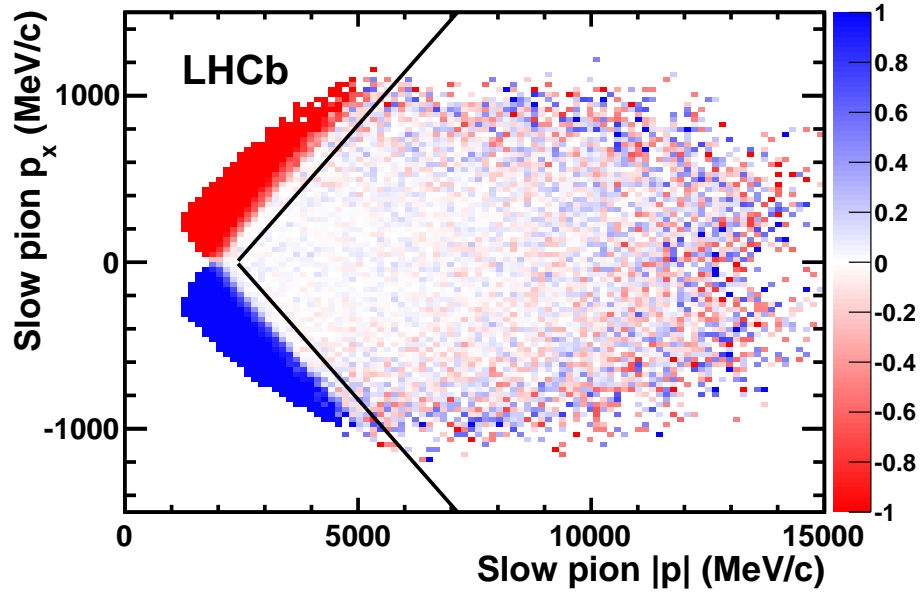


Figure 7: Raw asymmetry in bins of  $p_x$  vs  $p$  for reconstructed  $D^{*\pm} \rightarrow D^0(K^+K^-)\pi^\pm$  candidates. The plot shows candidates with  $|p_y/p_z| > 0.02$ . The solid lines show the excluded regions with large value of raw asymmetry. The data were taken with down polarity of the dipole magnetic field.

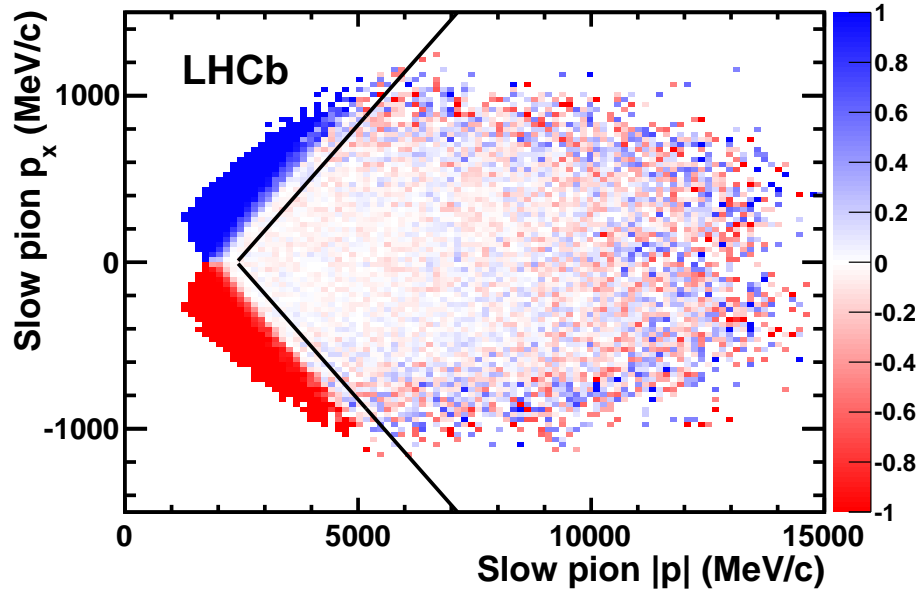


Figure 8: Raw asymmetry in bins of  $p_x$  vs  $p$  for reconstructed  $D^{*\pm} \rightarrow D^0(K^+K^-)\pi^\pm$  candidates. The plot shows candidates with  $|p_y/p_z| > 0.02$ . The solid lines show the excluded regions with large value of raw asymmetry. The data were taken with up polarity of the dipole magnetic field.

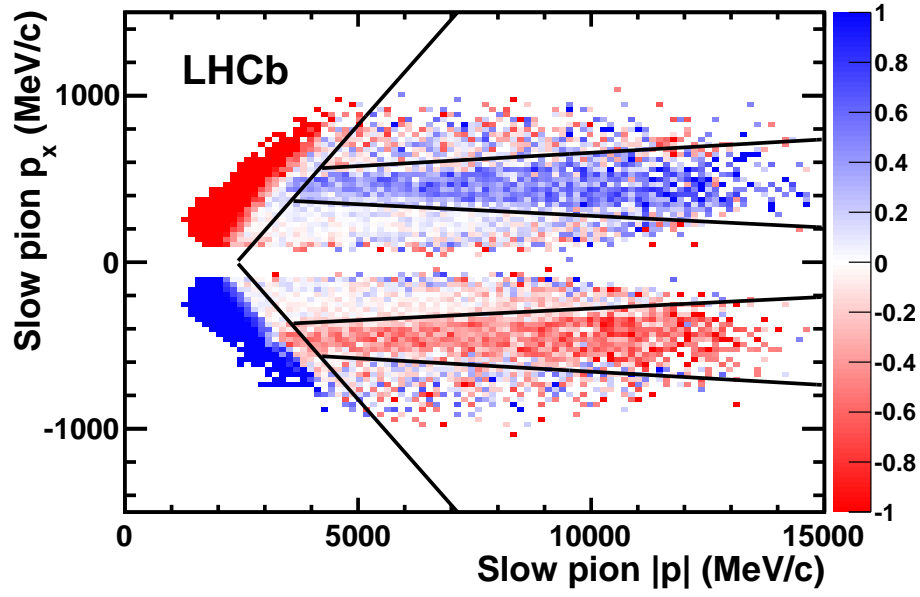


Figure 9: Raw asymmetry in bins of  $p_x$  vs  $p$  for reconstructed  $D^{*\pm} \rightarrow D^0(K^+K^-)\pi^\pm$  candidates. The plot shows candidates with  $|p_y/p_z| < 0.02$ . The solid lines show the excluded regions with large value of raw asymmetry. The data were taken with down polarity of the dipole magnetic field.

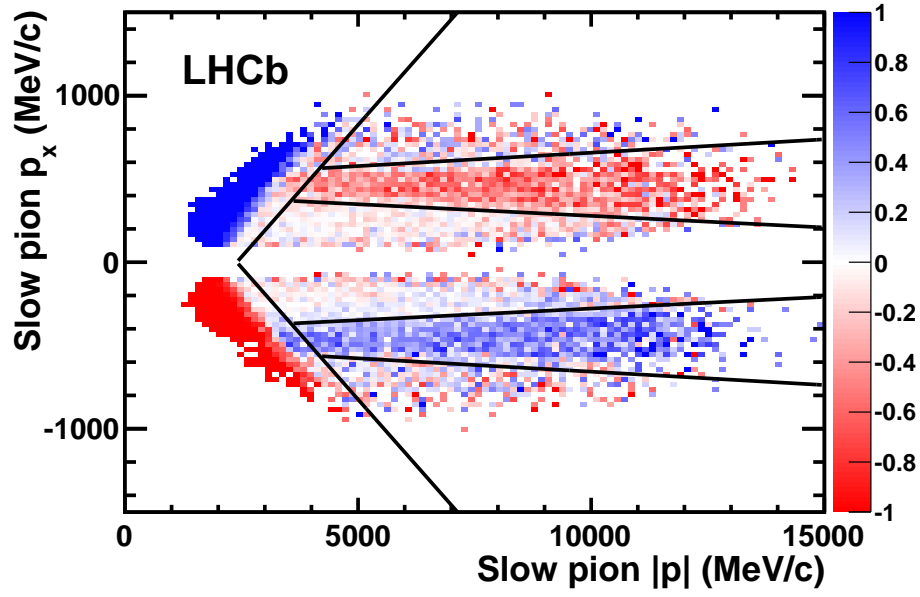


Figure 10: Raw asymmetry in bins of  $p_x$  vs  $p$  for reconstructed  $D^{*\pm} \rightarrow D^0(K^+K^-)\pi^\pm$  candidates. The plot shows candidates with  $|p_y/p_z| < 0.02$ . The solid lines show the excluded regions with large value of raw asymmetry. The data were taken with up polarity of the dipole magnetic field.

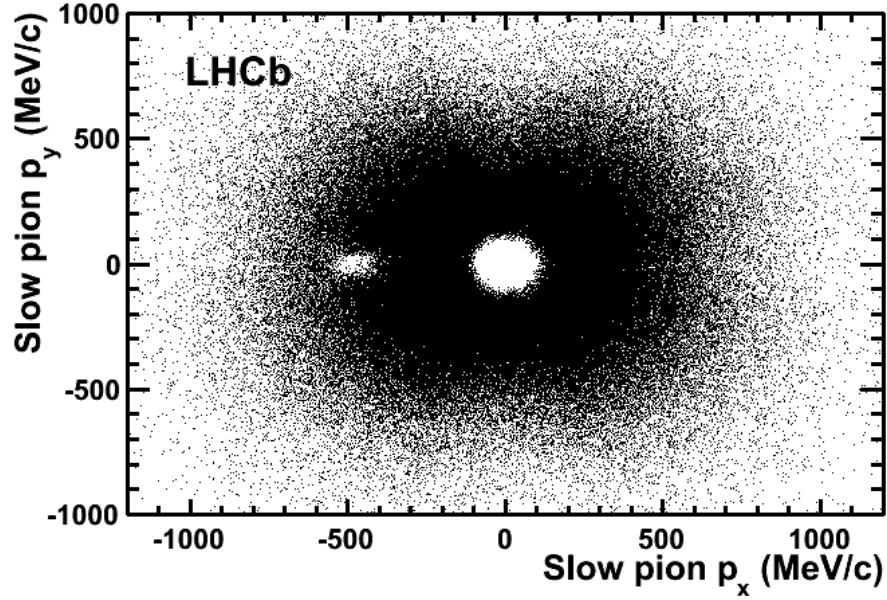


Figure 11: Scatterplot of  $(p_x, p_y)$  for reconstructed  $D^{*\pm} \rightarrow D^0(K^+K^-)\pi^\pm$  candidates. Only  $D^{*-}$  candidates are shown. The beam pipe acceptance is shown as a hole around  $(0,0)$  and as a depletion around  $(-500,0)$  where the slow pions are swept by the magnetic field into the beampipe in the downstream tracking station and hence has reduced efficiency. The data were taken with down polarity of the dipole magnetic field.



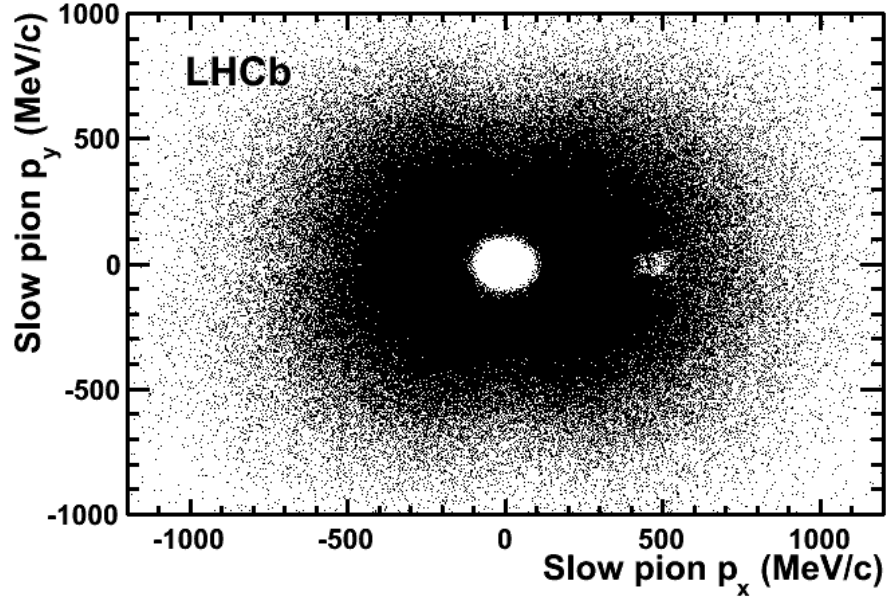


Figure 12: Scatterplot of  $(p_x, p_y)$  for reconstructed  $D^{*\pm} \rightarrow D^0(K^+K^-)\pi^\pm$  candidates. Only  $D^{*+}$  candidates are shown. The beam pipe acceptance is shown as a hole around  $(0,0)$  and as a depletion around  $(0, +500)$  where the soft pions are swept by the magnetic field into the beampipe in the downstream tracking station and hence has reduced efficiency. The data were taken with down polarity of the dipole magnetic field.